

Simple and Effective Masked Diffusion Language Models

Anonymous Authors¹

Abstract

While diffusion models excel at generating high-quality images, prior work reports a significant performance gap between diffusion and autoregressive (AR) methods on language modeling. In this work, we show that simple masked discrete diffusion is more performant than previously thought. We apply an effective training recipe that improves the performance of masked diffusion models and derive a simplified, Rao-Blackwellized objective that results in additional improvements. Our objective has a simple form—it is a mixture of classical masked language modeling losses—and can be used to train encoder-only language models that admit efficient samplers, including ones that can generate arbitrary lengths of text semi-autoregressively like a traditional language model. On language modeling benchmarks, a range of masked diffusion models trained with modern engineering practices achieves a new state-of-the-art among diffusion models, and approaches AR perplexity.

1. Introduction

In this work we describe (1) a simple masked diffusion language modeling (MDLM) framework with a well-engineered implementation that outperforms all existing diffusion models across language modeling benchmarks (LM1B (Chelba et al., 2014), OWT (Gokaslan et al., 2019), DNA (Schiff et al., 2024)), and that significantly improves the performance of existing baselines (Austin et al., 2021; He et al., 2022). Our MDLM framework implements (2a) a substitution-based parameterization (SUBS) of the reverse unmasking diffusion process; SUBS allows us to derive (2b) a simple, continuous-time, Rao-Blackwellized objective that improves tightness and variance of the ELBO, further increasing performance. We complement MDLM with

¹Anonymous Institution, Anonymous City, Anonymous Region, Anonymous Country. Correspondence to: Anonymous Author <anon.email@domain.com>.

Preliminary work. Under review by the ICML 2024 Workshop on Accessible and Efficient Foundation Models for Biological Discovery. Do not distribute.

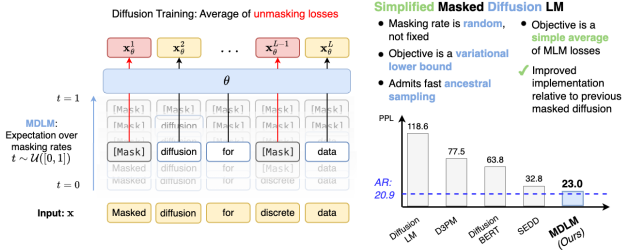


Figure 1: (Left) Our proposed masked diffusion language model (MDLM) is trained using a weighted average of masked cross entropy losses. (Top Right) In comparison to masked language models (MLM), MDLM’s objective correspond to a principled variational lower bound, and supports generation via ancestral sampling. (Bottom Right) Perplexity (PPL) on One Billion Words benchmark.

Table 1: Test perplexities (PPL; ↓) on LM1B. †Reported in He et al. (2022). Best diffusion value is bolded.

		Parameters	PPL (↓)
Ar	Transformer-X Base (Dai et al., 2019)	0.46B	23.5
	OmniNet _T (Tay et al., 2021)	100M	21.5
Dif	BERT-Mouth (Wang & Cho, 2019)	110M	≤142.89
	D3PM (absorb) (Austin et al., 2021)	70M	≤77.50
	Diffusion-LM (Li et al., 2022) [†]	80M	≤118.62
	DiffusionBert (He et al., 2022)	110M	≤63.78
	SEDD (Lou et al., 2023) (33B tokens)	110M	≤32.79
Ar (Retrained)	Transformer (33B tokens)	110M	22.32
	Transformer (330B tokens)	110M	20.86
Dif (Ours)	MDLM (33B tokens)	110M	≤27.04
	MDLM (330B tokens)	110M	≤ 23.00

(3) fast samplers that support semi-autoregressive (SAR) generation and outperform previous SAR models.

2. Background

2.1. Diffusion Models

Diffusion models are trained to iteratively undo a forward corruption process q that takes clean data \mathbf{x} drawn from the data distribution $q(\mathbf{x})$ and defines latent variables \mathbf{z}_t for $t \in [0, 1]$ that represent progressively noisy versions of \mathbf{x} (Ho et al., 2020; Sohl-Dickstein et al., 2015; Song et al., 2020). The standard forward process for continuous \mathbf{x} is

$$\mathbf{z}_t = \sqrt{\alpha_t} \cdot \mathbf{x} + \sqrt{1 - \alpha_t} \cdot \epsilon \quad (1)$$

where $\epsilon \sim \mathcal{N}(\mathbf{0}, \mathbf{I})$ and $(\alpha_t)_{t \in [0,1]}$ is a noise schedule, monotonically decreasing in t . The parameterized reverse diffusion model p_θ over \mathbf{x} and \mathbf{z}_t is trained to maximize a variational lower bound on log-likelihood (ELBO). Given a number of discretization steps T , defining $s(i) = (i-1)/T$ and $t(i) = i/T$, and using $D_{\text{KL}}[\cdot]$ to denote the Kullback–Leibler divergence, the ELBO equals (Sohl-Dickstein et al., 2015):

$$\mathbb{E}_q \left[\underbrace{\log p_\theta(\mathbf{x} | \mathbf{z}_{t(0)})}_{\mathcal{L}_{\text{recons}}} - \underbrace{\sum_{i=1}^T D_{\text{KL}}[q(\mathbf{z}_{s(i)} | \mathbf{z}_{t(i)}, \mathbf{x}) \| p_\theta(\mathbf{z}_{s(i)} | \mathbf{z}_{t(i)})]}_{\mathcal{L}_{\text{diffusion}}} \right] - \underbrace{D_{\text{KL}}[q(\mathbf{z}_{t(T)} | \mathbf{x}) \| p_\theta(\mathbf{z}_{t(T)})]}_{\mathcal{L}_{\text{prior}}} \quad (2)$$

For brevity, we drop i from $t(i)$ and $s(i)$ below; in general, s will denote the time step before t .

3. Simple Masked Diffusion Models

While previous work on discrete diffusion supports general forward processes (e.g., general Q_t in D3PM), absorbing state (i.e., masking) diffusion consistently achieves the best performance (Austin et al., 2021; Lou et al., 2023). In this work, instead of supporting general noise processes, we focus on masking and derive tight Rao-Blackwellized objectives that outperform general approaches and do not require CTMC theory. We denote our overall approach as masked diffusion (MDLM in the context of language models).

Notation. We denote scalar discrete random variables with K categories as ‘one-hot’ column vectors and define $\mathcal{V} \in \{\mathbf{x} \in \{0,1\}^K : \sum_{i=1}^K x_i = 1\}$ as the set of all such vectors. Define $\text{Cat}(\cdot; \boldsymbol{\pi})$ as the categorical distribution over K classes with probabilities given by $\boldsymbol{\pi} \in \Delta^K$, where Δ^K denotes the K -simplex. We also assume that the K -th category corresponds to a special [MASK] token and let $\mathbf{m} \in \mathcal{V}$ be the one-hot vector for this mask, i.e., $\mathbf{m}_K = 1$. Additionally, let $\mathbf{1} = \{1\}^K$ and $\langle \mathbf{a}, \mathbf{b} \rangle$ and $\mathbf{a} \odot \mathbf{b}$ respectively denote the dot and Hadamard products between two vectors \mathbf{a} and \mathbf{b} .

3.1. Interpolating Discrete Diffusion

We restrict our attention to forward processes q that interpolate between clean data $\mathbf{x} \in \mathcal{V}$ and a target distribution $\text{Cat}(\cdot; \boldsymbol{\pi})$, forming a direct extension of Gaussian diffusion in (1) given as:

$$q(\mathbf{z}_t | \mathbf{x}) = \text{Cat}(\mathbf{z}_t; \alpha_t \mathbf{x} + (1 - \alpha_t) \boldsymbol{\pi}), \quad (3)$$

where $\alpha_t \in [0,1]$ is a strictly decreasing function in t , with $\alpha_0 = 1$ and $\alpha_1 = 0$. This implies transition probabilities $q(\mathbf{z}_t | \mathbf{z}_s) = \text{Cat}(\mathbf{z}_t; \alpha_{t|s} \mathbf{z}_t + (1 - \alpha_{t|s}) \mathbf{1} \boldsymbol{\pi}^\top \mathbf{z}_t)$ where $\alpha_{t|s} = \alpha_t / \alpha_s$ and $q(\mathbf{z}_s | \mathbf{z}_t, \mathbf{x})$ is given as:

$$\text{Cat} \left(\mathbf{z}_s; \frac{[\alpha_{t|s} \mathbf{z}_t + (1 - \alpha_{t|s}) \mathbf{1} \boldsymbol{\pi}^\top \mathbf{z}_t] \odot [\alpha_s \mathbf{x} + (1 - \alpha_s) \boldsymbol{\pi}]}{\alpha_t \mathbf{z}_t^\top \mathbf{x} + (1 - \alpha_t) \mathbf{z}_t^\top \boldsymbol{\pi}} \right) \quad (4)$$

See Suppl. 14 for details. While (3) and (4) represent a special case of the more general diffusion processes proposed in D3PM (Austin et al., 2021), we show below that they yield a simplified variational lower bound objective and admit straightforward continuous time extensions.

3.2. Masked Diffusion

Forward Masking Process In masked (i.e., absorbing state) diffusion, we set $\boldsymbol{\pi} = \mathbf{m}$. At each noising step, the input \mathbf{x} transitions to a ‘masked’ state \mathbf{m} with a probability increasing in t . If an input transitions to \mathbf{m} at any time t' , it will remain in this state for all $t > t'$: $q(\mathbf{z}_t | \mathbf{z}_{t'} = \mathbf{m}) = \text{Cat}(\mathbf{z}_t; \mathbf{m})$. The marginal of the forward process (3) is given by $q(\mathbf{z}_t | \mathbf{x}) = \alpha_t \mathbf{x} + (1 - \alpha_t) \mathbf{m}$. Using properties of the masking process, the posterior $q(\mathbf{z}_s | \mathbf{z}_t, \mathbf{x})$ simplifies (4); see Suppl. A:

$$q(\mathbf{z}_s | \mathbf{z}_t, \mathbf{x}) = \begin{cases} \text{Cat}(\mathbf{z}_s; \mathbf{z}_t) & \mathbf{z}_t \neq \mathbf{m}, \\ \text{Cat} \left(\mathbf{z}_s; \frac{(1 - \alpha_s) \mathbf{m} + (\alpha_s - \alpha_t) \mathbf{x}}{1 - \alpha_t} \right) & \mathbf{z}_t = \mathbf{m}. \end{cases} \quad (5)$$

Reverse Unmasking Process: SUBS Parameterization

The reverse process inverts the noise process defined by q . We consider both a finite number of steps T , as well as a continuous time model corresponding to $T \rightarrow \infty$. We begin with the discrete-time case for which the generative model is expressed as $p_\theta(\mathbf{x}) = \int_{\mathbf{z}} p_\theta(\mathbf{z}_1) p_\theta(\mathbf{x} | \mathbf{z}_0) \prod_{i=1}^T p_\theta(\mathbf{z}_s | \mathbf{z}_t) d\mathbf{z}_{0:T}$. We introduce a model $\mathbf{x}_\theta(\mathbf{z}_t, t) : \mathcal{V} \times [0,1] \rightarrow \Delta^K$ that approximates \mathbf{x} with a neural network. The specific parameterization for $p_\theta(\mathbf{z}_s | \mathbf{z}_t)$ that we use is

$$p_\theta(\mathbf{z}_s | \mathbf{z}_t) = \begin{cases} \text{Cat}(\mathbf{z}_s; \mathbf{z}_t), & \mathbf{z}_t \neq \mathbf{m}, \\ \text{Cat} \left(\mathbf{z}_s; \frac{(1 - \alpha_s) \mathbf{m} + (\alpha_s - \alpha_t) \mathbf{x}_\theta(\mathbf{z}_t, t)}{1 - \alpha_t} \right). & \mathbf{z}_t = \mathbf{m}. \end{cases} \quad (6)$$

In order for $p_\theta(\mathbf{z}_s | \mathbf{z}_t)$ to be a valid probability, $\mathbf{x}_\theta(\mathbf{z}_t, t)$ must satisfy two requirements. We implement these as substitutions to the output of $\mathbf{x}_\theta(\mathbf{z}_t, t)$, hence we call our parameterization SUBS.

Zero Masking Probabilities First, notice that by definition, $\langle \mathbf{x}, \mathbf{m} \rangle = 0$. For this reason, we design the denoising network such that $\langle \mathbf{x}_\theta(\mathbf{z}_t), \mathbf{m} \rangle = 0$, i.e., we substitute the logit index corresponding to the [MASK] token with $-\infty$. This property enables the simplified expression of (6) (Suppl. A.3.2) and ensures that case 2 in (6) is a valid probability.

Carry-Over Unmasking Second, if \mathbf{z}_t is unmasked, then we desire $\mathbf{x}_\theta(\mathbf{z}_t, t) = \mathbf{z}_t$, i.e., unmasked latents are ‘carried over’. We accomplish this by substituting the output of our network to simply copy unmasked inputs. This ensures that case 1 in (6) always holds, and furthermore reduces $\mathcal{L}_{\text{recons}}$ to 0.

3.3. Rao-Blackwellized Likelihood Bounds

Recall from (2) that the diffusion training objective has the form $\mathcal{L}_{\text{recons}} + \mathcal{L}_{\text{diffusion}} + \mathcal{L}_{\text{prior}}$. For the simplified reverse process in (6), the discrete-time diffusion loss for finite T simplifies to (Suppl. B.1):

$$\mathcal{L}_{\text{diffusion}} = \sum_{i=1}^T \mathbb{E}_q \left[\frac{\alpha_{t(i)} - \alpha_{s(i)}}{1 - \alpha_{t(i)}} \log \langle \mathbf{x}_\theta(\mathbf{z}_{t(i)}), \mathbf{x} \rangle \right]. \quad (7)$$

Note that this objective is simpler and more well-behaved than the expression one would obtain for $D_{\text{KL}}(q(\mathbf{z}_s | \mathbf{z}_t, \mathbf{x}) \| p_\theta(\mathbf{z}_s | \mathbf{z}_t))$ under the parameterization induced by using $p_\theta(\mathbf{z}_s | \mathbf{z}_t) = q(\mathbf{z}_s | \mathbf{z}_t, \mathbf{x} = \mathbf{x}_\theta(\mathbf{z}_t, t))$ from (4), which is similar to what is used by D3PM (Austin et al., 2021) (see Suppl. 27):

$$\left[\frac{\alpha_s - \alpha_t}{1 - \alpha_t} \log \frac{\alpha_t \langle \mathbf{x}_\theta(\mathbf{z}_t), \mathbf{m} \rangle + (1 - \alpha_t)}{(1 - \alpha_t) \langle \mathbf{x}_\theta(\mathbf{z}_t), \mathbf{x} \rangle} + \frac{1 - \alpha_s}{1 - \alpha_t} \log \frac{(1 - \alpha_s) (\alpha_t \langle \mathbf{x}_\theta(\mathbf{z}_t), \mathbf{m} \rangle + (1 - \alpha_t))}{(1 - \alpha_t) (\alpha_s \langle \mathbf{x}_\theta(\mathbf{z}_t), \mathbf{m} \rangle + (1 - \alpha_s))} \right] \langle \mathbf{z}_t, \mathbf{m} \rangle. \quad (8)$$

We refer to the process of obtaining (7) in lieu of (8) as a form of Rao-Blackwellization.

3.4. Continuous-Time Likelihood Bounds

Previous works have shown empirically and mathematically that increasing the number of steps T yields a tighter approximation to the ELBO (Kingma et al., 2021). Following a similar argument, we form a continuous extension of (7) by taking $T \rightarrow \infty$ (see Suppl. B.2), which yields

$$\mathcal{L}_{\text{diffusion}}^\infty = \mathbb{E}_q \int_{t=0}^{t=1} \frac{\alpha'_t}{1 - \alpha_t} \log \langle \mathbf{x}_\theta(\mathbf{z}_t), \mathbf{x} \rangle dt \quad (9)$$

3.5. Masked Diffusion Language Models

Next, we apply masked diffusion to language modeling over sequences $\mathbf{x}^{1:L}$ of L tokens, with \mathbf{x}^ℓ denoting the ℓ -th token. We make the assumption that the forward noising process is applied independently across a sequence and that, conditioned on a sequence of latents $\mathbf{z}_t^{1:L}$, the denoising process factorizes independently across tokens, i.e., $p_\theta(\mathbf{z}_s^{1:L} | \mathbf{z}_t^{1:L}) = \prod_{\ell=1}^L p_\theta(\mathbf{z}_s^\ell | \mathbf{z}_t^{1:L})$. Thus, we use a single model to compute $\mathbf{x}_\theta^\ell(\mathbf{z}_t^{1:L}, t)$ for each ℓ from a masked sequence \mathbf{z}_t , optimizing:

$$\mathcal{L}_{\text{diffusion}}^\infty = \mathbb{E}_q \int_{t=0}^{t=1} \frac{\alpha'_t}{1 - \alpha_t} \sum_{\ell} \log \langle \mathbf{x}_\theta^\ell(\mathbf{z}_t), \mathbf{x}^\ell \rangle dt \quad (10)$$

Interestingly, our objective has a simple form: it is the weighted average of masked language modeling (MLM) losses (Devlin et al., 2018). Thus our work establishes a connection between generative diffusion models and encoder-only BERT models. Our objective enables principled selection of a (randomized) masking rate, and also endows BERT-style models with principled generation capabilities, see Sec. 6.

4. Inference and Sampling in Masked Diffusion Language Models

4.1. Efficient Ancestral Sampling

To generate a sequence of length L , the reverse diffusion process starts with the sequence $\mathbf{z}_{t=1}^{1:L}$ where $\mathbf{z}_{t=1}^\ell = \mathbf{m}$, $\forall \ell \in \{1, \dots, L\}$. Then the subsequent latents, $\mathbf{z}_t^{1:L}$ are generated by discretizing the reverse diffusion process with some finite T . Given $\mathbf{z}_t^{1:L}$, we construct $\mathbf{z}_s^{1:L}$ by sampling each token \mathbf{z}_s^ℓ independently from the distribution $p_\theta(\mathbf{z}_s^\ell | \mathbf{z}_t^{1:L})$ given in (6).

4.2. Semi-Autoregressive Masked Diffusion Language Models

Our method also admits an effective semi-autoregressive (SAR) decoding method that allows the model to generate sequences of arbitrary length. Let $\tilde{\mathbf{x}}^{1:L}$ represent the output from sampling a sequence of L tokens using the reverse diffusion process described above. To generate additional $L' < L$ tokens, we propose a generation algorithm in which the latter $L - L'$ tokens $\tilde{\mathbf{x}}^{L':L-L'}$ are used as a prefix for an additional round of generation. Given the carry-over unmasking described in Sec. 3.2, these prefix tokens will simply be copied over at each decoding step. The remaining tokens are generated as above with $\mathbf{z}_s^\ell \sim p_\theta(\mathbf{z}_s^\ell | \mathbf{z}_t^{L':L+L'})$ for all $\ell \in \{L+1, \dots, L+L'\}$, with $\mathbf{z}_t^{L':L-L'}$ initialized to $\tilde{\mathbf{x}}^{L':L-L'}$ as opposed to being initialized as masked tokens \mathbf{m} . At the end of this process, we have produced $L + L'$ tokens $\text{concat}[\tilde{\mathbf{x}}^{1:L}, \tilde{\mathbf{x}}^{L+1:L+L'}]$, where $\text{concat}[\cdot]$ denotes concatenation along the sequence length dimension. This process can repeat indefinitely, with the prefix shifted for every new round of generation.

5. Experiments

The experiment setup is described in Suppl. C.1

5.1. Masked Diffusion Language Models

Likelihood Evaluation On LM1B, MDLM outperforms all previous diffusion methods (Table 1). Compared to the SEDD baseline reported by Lou et al. (2023), trained for 66B tokens, MDLM, which we train for the same amount, achieves a 17% improvement on the perplexity bound. Finally, MDLM gets within 14% of an AR baseline and continues to improve with more training. We see the same trend for models trained on OWT, a larger dataset, shown in Table 9 – MDLM outperforms prior diffusion methods, closing the gap towards AR models. Results on OWT time step conditioning are in Table 6, Suppl. C.5 where we find that models trained with and without time conditioning attain similar perplexities. Additionally, Figure 2 demonstrates the reduced variance we achieve from our objective, when compared to previous masked diffusion models, such as SEDD (Lou et al., 2023).

Table 2: Genomic Benchmarks. Top-1 accuracy (\uparrow) across 5-fold cross-validation (CV) for a pre-trained AR Mamba, and pre-trained Caduceus model fine-tuned with different diffusion parameterizations. Best values per task are bolded and second best are italicized. Error bars indicate difference between maximum and minimum values across 5 random seeds used for CV.

Model / Fine-Tuning (Params)	Mamba / AR (465K)	Caduceus / MLM (467K)	Caduceus / Plaid (507k)	Caduceus / SEDD (467k)	Caduceus / MDLM (467k)
Mouse Enhancers	0.763 $\{\pm 0.008\}$	0.810 $\{\pm 0.016\}$	0.745 $\{\pm 0.079\}$	0.784 $\{\pm 0.058\}$	<i>0.795</i> $\{\pm 0.029\}$
Coding vs. Intergenic	0.897 $\{\pm 0.004\}$	0.913 $\{\pm 0.003\}$	<i>0.908</i> $\{\pm 0.003\}$	0.913 $\{\pm 0.005\}$	0.913 $\{\pm 0.003\}$
Human vs. Worm	0.967 $\{\pm 0.002\}$	<i>0.970</i> $\{\pm 0.002\}$	0.971 $\{\pm 0.001\}$	<i>0.970</i> $\{\pm 0.003\}$	<i>0.970</i> $\{\pm 0.003\}$
Human Enhancers Cohn	0.734 $\{\pm 0.027\}$	0.737 $\{\pm 0.001\}$	<i>0.743</i> $\{\pm 0.010\}$	0.746 $\{\pm 0.015\}$	<i>0.743</i> $\{\pm 0.016\}$
Human Enhancer Ensembl	0.856 $\{\pm 0.003\}$	0.907 $\{\pm 0.000\}$	0.885 $\{\pm 0.003\}$	<i>0.905</i> $\{\pm 0.006\}$	0.899 $\{\pm 0.004\}$
Human Regulatory	0.861 $\{\pm 0.008\}$	0.874 $\{\pm 0.003\}$	<i>0.868</i> $\{\pm 0.010\}$	0.828 $\{\pm 0.037\}$	<i>0.868</i> $\{\pm 0.004\}$
Human OCR Ensembl	0.806 $\{\pm 0.005\}$	<i>0.821</i> $\{\pm 0.000\}$	0.820 $\{\pm 0.004\}$	0.816 $\{\pm 0.008\}$	0.823 $\{\pm 0.008\}$
Human NonTATA Promoters	0.926 $\{\pm 0.008\}$	<i>0.935</i> $\{\pm 0.014\}$	<i>0.935</i> $\{\pm 0.01007\}$	<i>0.935</i> $\{\pm 0.014\}$	0.940 $\{\pm 0.007\}$

Zero-Shot Likelihood Evaluation We also explore models’ ability to generalize by taking models trained on OWT and evaluating how well they model unseen datasets. MDLM consistently outperforms the SEDD diffusion parameterization on all datasets. In some cases, e.g., for Lambada and Scientific Papers, MDLM attains better perplexity than AR. Details in Suppl. C.6.

Downstream Task Evaluation In Table 8, we find that BERT fine-tuned with MDLM to be a generative model results in strong perplexities while preserving performance on downstream tasks.

Semi-Autoregressive Modeling To test the SAR decoding algorithm presented in Sec. 4.2, we compare to SSD-LM (Han et al., 2022). In Table 11, we find that in addition to achieving better generative perplexity, MDLM enables ~ 25 - 30 x faster SAR decoding relative to SSD-LM (details in Suppl. C.10).

5.2. Masked Diffusion DNA Models

We also explore the use of our generative formulation in conjunction with Structured State Space models (Gu et al., 2021). Namely, we build on the recently proposed Caduceus (Schiff et al., 2024) model, which uses as a backbone the data-dependent SSM Mamba block (Gu & Dao, 2023). We pre-train the encoder-only Caduceus (Schiff et al., 2024), which is an MLM, on the HG38 human reference genome (Consortium, 2009) and perform fine-tuning using our diffusion parameterization. We use a context length of 1024 tokens and follow Schiff et al. (2024) for the experimental setup, other than learning rate which was reduced to $1e-3$. See Suppl. I.4 for full experimental details. We assess both generative performance using perplexity and downstream performance on Genomics Benchmarks (Grešová et al., 2023) across language diffusion paradigms and AR models.

Generative Performance We fine-tune the Caduceus MLM across diffusion parameterizations and compare perplexities against AR models. We report perplexity values

in Table 3. MDLM outperforms all other diffusion language modeling schemes.

Table 3: Test perplexities (PPL; \downarrow) of generative fine-tuning of the Caduceus MLM (Schiff et al., 2024) on the HG38 reference genome. Best diffusion model values are bolded. Error bars indicate the difference between the maximum and minimum values across 5 random seeds used for fine-tuning. \dagger denotes retrained models.

		Params	PPL (\downarrow)
AR^\dagger	Mamba	465K	$3.067 \pm .0104$
	HyenaDNA	433K	$3.153 \pm .001$
Dif^\dagger	Plaid	507K	$\leq 3.240 \pm .005$
	SEDD	467K	$\leq 3.216 \pm .003$
$Dif(Ours)$	MDLM	467K	$\leq \mathbf{3.199} \pm .010$

Downstream Task Fine-tuning We perform downstream evaluation with the Genomics Benchmarks (Grešová et al., 2023), a recently proposed benchmark with eight regulatory element classification tasks. As shown in Table 2, our generative fine-tuning paradigm preserves or improves upon downstream performance from MLM pre-training. Absorbing-state diffusion methods outperform Plaid across tasks except for the simplest task Human vs. Worm, where all methods have roughly the same performance. For tasks where the input is a biased subsample of the full genome, we observe that the correlation between perplexity and downstream performance is weaker; see Suppl. I.4.

6. Conclusion

Conclusion In this work, we explore masked diffusion. With a well-engineered implementation that supports a simple variational objective, we attain state-of-the-art diffusion perplexities on language benchmarks and demonstrate how to efficiently convert BERT-style encoders into generative models.

References

- Jacob Austin, Daniel D Johnson, Jonathan Ho, Daniel Tarlow, and Rianne Van Den Berg. Structured denoising diffusion models in discrete state-spaces. *Advances in Neural Information Processing Systems*, 34:17981–17993, 2021.
- Žiga Avsec, Vikram Agarwal, Daniel Visentin, Joseph R Ledsam, Agnieszka Grabska-Barwinska, Kyle R Taylor, Yannis Assael, John Jumper, Pushmeet Kohli, and David R Kelley. Effective gene expression prediction from sequence by integrating long-range interactions. *Nature methods*, 18(10):1196–1203, 2021.
- Andrew Campbell, Joe Benton, Valentin De Bortoli, Thomas Rainforth, George Deligiannidis, and Arnaud Doucet. A continuous time framework for discrete denoising models. *Advances in Neural Information Processing Systems*, 35: 28266–28279, 2022.
- Ciprian Chelba, Tomas Mikolov, Mike Schuster, Qi Ge, Thorsten Brants, Phillipp Koehn, and Tony Robinson. One billion word benchmark for measuring progress in statistical language modeling, 2014.
- Ting Chen, Ruixiang Zhang, and Geoffrey Hinton. Analog bits: Generating discrete data using diffusion models with self-conditioning. *arXiv preprint arXiv:2208.04202*, 2022.
- Arman Cohan, Franck Dernoncourt, Doo Soon Kim, Trung Bui, Seokhwan Kim, Walter Chang, and Nazli Goharian. A discourse-aware attention model for abstractive summarization of long documents. *Proceedings of the 2018 Conference of the North American Chapter of the Association for Computational Linguistics: Human Language Technologies, Volume 2 (Short Papers)*, 2018. doi: 10.18653/v1/n18-2097. URL <http://dx.doi.org/10.18653/v1/n18-2097>.
- Genome Reference Consortium. Genome reference consortium human build 37 (grch37). *Database (GenBank or RefSeq)*, 2009.
- Zihang Dai, Zhilin Yang, Yiming Yang, Jaime Carbonell, Quoc V Le, and Ruslan Salakhutdinov. Transformer-xl: Attentive language models beyond a fixed-length context. *arXiv preprint arXiv:1901.02860*, 2019.
- Jacob Devlin, Ming-Wei Chang, Kenton Lee, and Kristina Toutanova. Bert: Pre-training of deep bidirectional transformers for language understanding. *arXiv preprint arXiv:1810.04805*, 2018.
- Sander Dieleman, Laurent Sartran, Arman Roshannai, Nikolay Savinov, Yaroslav Ganin, Pierre H Richemond, Arnaud Doucet, Robin Strudel, Chris Dyer, Conor Durkan, et al. Continuous diffusion for categorical data. *arXiv preprint arXiv:2211.15089*, 2022.
- Aaron Gokaslan, Vanya Cohen, Ellie Pavlick, and Stefanie Tellex. Openwebtext corpus. <http://SkyLion007.github.io/OpenWebTextCorpus>, 2019.
- Katarína Grešová, Vlastimil Martinek, David Čechák, Petr Šimeček, and Panagiotis Alexiou. Genomic benchmarks: a collection of datasets for genomic sequence classification. *BMC Genomic Data*, 24(1):25, 2023.
- Albert Gu and Tri Dao. Mamba: Linear-time sequence modeling with selective state spaces. *arXiv preprint arXiv:2312.00752*, 2023.
- Albert Gu, Karan Goel, and Christopher Ré. Efficiently modeling long sequences with structured state spaces. *arXiv preprint arXiv:2111.00396*, 2021.
- Ishaan Gulrajani and Tatsunori B Hashimoto. Likelihood-based diffusion language models. *Advances in Neural Information Processing Systems*, 36, 2024.
- Xiaochuang Han, Sachin Kumar, and Yulia Tsvetkov. Ssd-lm: Semi-autoregressive simplex-based diffusion language model for text generation and modular control. *arXiv preprint arXiv:2210.17432*, 2022.
- Zhengfu He, Tianxiang Sun, Kuanning Wang, Xuanjing Huang, and Xipeng Qiu. Diffusionbert: Improving generative masked language models with diffusion models. *arXiv preprint arXiv:2211.15029*, 2022.
- Jonathan Ho, Ajay Jain, and Pieter Abbeel. Denoising diffusion probabilistic models. *Advances in neural information processing systems*, 33:6840–6851, 2020.
- Diederik Kingma, Tim Salimans, Ben Poole, and Jonathan Ho. Variational diffusion models. *Advances in neural information processing systems*, 34:21696–21707, 2021.
- Xiang Li, John Thickstun, Ishaan Gulrajani, Percy S Liang, and Tatsunori B Hashimoto. Diffusion-lm improves controllable text generation. *Advances in Neural Information Processing Systems*, 35:4328–4343, 2022.
- Aaron Lou, Chenlin Meng, and Stefano Ermon. Discrete diffusion language modeling by estimating the ratios of the data distribution. *arXiv preprint arXiv:2310.16834*, 2023.
- Justin Lovelace, Varsha Kishore, Chao Wan, Eliot Shekhtman, and Kilian Q Weinberger. Latent diffusion for language generation. *Advances in Neural Information Processing Systems*, 36, 2024.
- Vincent Mallet and Jean-Philippe Vert. Reverse-complement equivariant networks for dna sequences. *Advances in neural information processing systems*, 34:13511–13523, 2021.

- 275 Mitch Marcus, Beatrice Santorini, and Mary Ann
276 Marcinkiewicz. Building a large annotated corpus of
277 english: The penn treebank. *Computational linguistics*,
278 19(2):313–330, 1993.
- 279 Stephen Merity, Caiming Xiong, James Bradbury, and
280 Richard Socher. Pointer sentinel mixture models, 2016.
- 282 Eric Nguyen, Michael Poli, Marjan Faizi, Armin Thomas,
283 Michael Wornow, Callum Birch-Sykes, Stefano Massaroli,
284 Aman Patel, Clayton Rabideau, Yoshua Bengio, et al.
285 Hyenadna: Long-range genomic sequence modeling
286 at single nucleotide resolution. *Advances in neural
287 information processing systems*, 36, 2024.
- 288 Denis Paperno, Germán Kruszewski, Angeliki Lazari-
289 dou, Ngoc Quan Pham, Raffaella Bernardi, Sandro
290 Pezzelle, Marco Baroni, Gemma Boleda, and Raquel
291 Fernandez. The LAMBADA dataset: Word prediction
292 requiring a broad discourse context. In *Proceedings
293 of the 54th Annual Meeting of the Association for
294 Computational Linguistics (Volume 1: Long Papers)*,
295 pp. 1525–1534, Berlin, Germany, August 2016. Asso-
296 ciation for Computational Linguistics. URL <http://www.aclweb.org/anthology/P16-1144>.
- 299 William Peebles and Saining Xie. Scalable diffusion models
300 with transformers. In *Proceedings of the IEEE/CVF
301 International Conference on Computer Vision*, pp.
302 4195–4205, 2023.
- 303 Jacob Portes, Alex Trott, Sam Havens, Daniel King, Abhinav
304 Venigalla, Moin Nadeem, Nikhil Sardana, Daya Khudia,
305 and Jonathan Frankle. Mosaicbert: A bidirectional
306 encoder optimized for fast pretraining, 2024.
- 308 Ofir Press, Noah A. Smith, and Mike Lewis. Train short,
309 test long: Attention with linear biases enables input length
310 extrapolation, 2022.
- 312 Alec Radford, Jeff Wu, Rewon Child, David Luan, Dario
313 Amodei, and Ilya Sutskever. Language models are
314 unsupervised multitask learners. 2019.
- 315 Colin Raffel, Noam Shazeer, Adam Roberts, Katherine Lee,
316 Sharan Narang, Michael Matena, Yanqi Zhou, Wei Li, and
317 Peter J. Liu. Exploring the limits of transfer learning with
318 a unified text-to-text transformer. *J. Mach. Learn. Res.*,
319 21(1), jan 2020. ISSN 1532-4435.
- 321 Yair Schiff, Chia-Hsiang Kao, Aaron Gokaslan, Tri
322 Dao, Albert Gu, and Volodymyr Kuleshov. Caduceus:
323 Bi-directional equivariant long-range dna sequence
324 modeling. *arXiv preprint arXiv:2403.03234*, 2024.
- 325 Jascha Sohl-Dickstein, Eric Weiss, Niru Maheswaranathan,
326 and Surya Ganguli. Deep unsupervised learning using
327 nonequilibrium thermodynamics. In *International confer-
328 ence on machine learning*, pp. 2256–2265. PMLR, 2015.
- 329 Yang Song and Stefano Ermon. Generative modeling by
estimating gradients of the data distribution. *Advances
in neural information processing systems*, 32, 2019.
- Yang Song, Jascha Sohl-Dickstein, Diederik P Kingma,
Abhishek Kumar, Stefano Ermon, and Ben Poole. Score-
based generative modeling through stochastic differential
equations. *arXiv preprint arXiv:2011.13456*, 2020.
- Robin Strudel, Corentin Tallec, Florent Althé, Yilun
Du, Yaroslav Ganin, Arthur Mensch, Will Grathwohl,
Nikolay Savinov, Sander Dieleman, Laurent Sifre, et al.
Self-conditioned embedding diffusion for text generation.
arXiv preprint arXiv:2211.04236, 2022.
- Jianlin Su, Yu Lu, Shengfeng Pan, Ahmed Murtadha,
Bo Wen, and Yunfeng Liu. Roformer: Enhanced
transformer with rotary position embedding. *arXiv
preprint arXiv:2104.09864*, 2021.
- Haoran Sun, Lijun Yu, Bo Dai, Dale Schuurmans, and
Hanjun Dai. Score-based continuous-time discrete
diffusion models. *arXiv preprint arXiv:2211.16750*, 2022.
- Yi Tay, Mostafa Dehghani, Vamsi Aribandi, Jai Gupta,
Philip M Pham, Zhen Qin, Dara Bahri, Da-Cheng Juan,
and Donald Metzler. Omninet: Omnidirectional represen-
tations from transformers. In *International Conference
on Machine Learning*, pp. 10193–10202. PMLR, 2021.
- Alex Wang and Kyunghyun Cho. Bert has a mouth, and
it must speak: Bert as a markov random field language
model. *arXiv preprint arXiv:1902.04094*, 2019.
- Alex Wang, Amanpreet Singh, Julian Michael, Felix
Hill, Omer Levy, and Samuel R. Bowman. GLUE: A
multi-task benchmark and analysis platform for natural
language understanding. In *International Conference
on Learning Representations*, 2019. URL <https://openreview.net/forum?id=rJ4km2R5t7>.
- Xiang Zhang, Junbo Jake Zhao, and Yann LeCun. Character-
level convolutional networks for text classification. In
NIPS, 2015.
- Hannah Zhou, Avanti Shrikumar, and Anshul Kundaje.
Towards a better understanding of reverse-complement
equivariance for deep learning models in genomics. In
Machine Learning in Computational Biology, pp. 1–33.
PMLR, 2022.

A. Discrete time ELBO

This section is organized as follows: First, we derive the expressions for the true posterior and the approximate posterior as outlined in Suppl. A.2. We then simplify these expressions specifically for the case of absorbing state diffusion in Suppl. A.3. Finally, we derive the expression for the ELBO for absorbing state diffusion in Suppl. A.3.3.

A.1. Discrete Diffusion Models

Applications of diffusion modeling to discrete data can be broken into two broad categories. First are works that embed discrete structures in continuous space and then perform the Gaussian diffusion defined above on these continuous representations (Chen et al., 2022; Dieleman et al., 2022; Gulrajani & Hashimoto, 2024; Han et al., 2022; Li et al., 2022; Lovelace et al., 2024; Strudel et al., 2022). More related to our method are works that define a diffusion process directly on discrete structures. D3PM (Austin et al., 2021) introduces a framework with a Markov forward process $q(\mathbf{z}_t | \mathbf{z}_{t-1}) = \text{Cat}(\mathbf{z}_t; Q_t \mathbf{z}_{t-1})$ defined by the multiplication of matrices Q_t over T discrete time steps. This process induces marginals

$$q(\mathbf{z}_t | \mathbf{x}) = \text{Cat}(\mathbf{z}_t; \bar{Q}_t \mathbf{x}) = \text{Cat}(\mathbf{z}_t; Q_t \cdot Q_{t-1} \cdots Q_1 \mathbf{x}) \quad (11)$$

that represent the discrete-state form of (1). Extending this formalism to continuous time (as in (1)) relies on continuous time Markov chain (CTMC) theory (Campbell et al., 2022). The CTMC framework in turns leads to generalizations of the score matching perspective on diffusion modeling (Song & Ermon, 2019) to discrete data (Lou et al., 2023; Sun et al., 2022). Notably, SEDD (Lou et al., 2023) connects score-based approaches with ELBO maximization, enabling performant likelihood-based training of score-based models.

A.2. Generic case

A.2.1. $q(\mathbf{z}_s | \mathbf{z}_t, \mathbf{x})$

Given the state transition matrix Q_t , prior $\boldsymbol{\pi}$, and the latent variables \mathbf{z}_s and \mathbf{z}_t , where $s < t$, the forward process defined in (11) has the following posterior (Austin et al., 2021):

$$q(\mathbf{z}_s | \mathbf{z}_t, \mathbf{x}) = \text{Cat} \left(\mathbf{z}_s; \frac{\bar{Q}_{t|s} \mathbf{z}_t \odot \bar{Q}_s^\top \mathbf{x}}{\mathbf{z}_t^\top \bar{Q}_t^\top \mathbf{x}} \right) \quad (12)$$

$$\bar{Q}_{t|s} = \alpha_{t|s} \mathbf{I}_n + (1 - \alpha_{t|s}) \mathbf{1} \boldsymbol{\pi}^\top \quad (13)$$

which we simplify to the following:

$$\begin{aligned} & q(\mathbf{z}_s | \mathbf{z}_t, \mathbf{x}) \\ &= \text{Cat} \left(\mathbf{z}_s; \frac{[\alpha_{t|s} \mathbf{I}_n + (1 - \alpha_{t|s}) \mathbf{1} \boldsymbol{\pi}^\top] \mathbf{z}_t \odot [\alpha_s \mathbf{I}_n + (1 - \alpha_s) \mathbf{1} \boldsymbol{\pi}^\top]^\top \mathbf{x}}{\mathbf{z}_t^\top [\alpha_t \mathbf{I}_n + (1 - \alpha_t) \mathbf{1} \boldsymbol{\pi}^\top]^\top \mathbf{x}} \right) \\ &= \text{Cat} \left(\mathbf{z}_s; \frac{[\alpha_{t|s} \mathbf{z}_t + (1 - \alpha_{t|s}) \mathbf{1} \boldsymbol{\pi}^\top \mathbf{z}_t] \odot [\alpha_s \mathbf{x} + (1 - \alpha_s) \boldsymbol{\pi}]}{\mathbf{z}_t^\top [\alpha_t \mathbf{x} + (1 - \alpha_t) \boldsymbol{\pi} \mathbf{1}^\top \mathbf{x}]} \right) \\ & \text{Using the property } \mathbf{1}^\top \mathbf{x} = 1 \text{ we get,} \\ &= \text{Cat} \left(\mathbf{z}_s; \frac{[\alpha_{t|s} \mathbf{z}_t + (1 - \alpha_{t|s}) \mathbf{1} \boldsymbol{\pi}^\top \mathbf{z}_t] \odot [\alpha_s \mathbf{x} + (1 - \alpha_s) \boldsymbol{\pi}]}{\alpha_t \mathbf{z}_t^\top \mathbf{x} + (1 - \alpha_t) \mathbf{z}_t^\top \boldsymbol{\pi}} \right). \end{aligned} \quad (14)$$

A.2.2. $p_\theta(\mathbf{z}_s | \mathbf{z}_t)$

Austin et al. (2021) approximate the reverse process in the following manner:

$$p_\theta(\mathbf{x}_s | \mathbf{x}_t) = q(\mathbf{z}_s | \mathbf{z}_t, \mathbf{x} = \mathbf{x}_\theta(\mathbf{z}_t, t)) = \text{Cat} \left(\mathbf{x}_s; \frac{\bar{Q}_{t|s} \mathbf{x}_t \odot \bar{Q}_s^\top \mathbf{x}_\theta(\mathbf{z}_t, t)}{\mathbf{x}_t^\top \bar{Q}_t^\top \mathbf{x}_\theta(\mathbf{z}_t, t)} \right). \quad (15)$$

where $\mathbf{x}_\theta(\mathbf{z}_t, t) : \mathcal{V} \times [0, 1] \rightarrow \Delta^K$ is an approximation for \mathbf{x} .

A.3. Absorbing state

For the absorbing state diffusion process we have $\pi = \mathbf{m}$.

A.3.1. $q(\mathbf{z}_s | \mathbf{z}_t, \mathbf{x})$

Since, $\mathbf{z}_t \in \{\mathbf{x}, \mathbf{m}\}$, takes only 2 values we consider the separate cases: $\mathbf{z}_t = \mathbf{x}$ and $\mathbf{z}_t = \mathbf{m}$.

Case 1. Consider the case $\mathbf{z}_t = \mathbf{x}$ i.e. \mathbf{z}_t is unmasked. From (14), we have the following:

$$\begin{aligned}
 & q(\mathbf{z}_s | \mathbf{z}_t = \mathbf{x}, \mathbf{x}) \\
 &= \text{Cat} \left(\mathbf{z}_s; \frac{[\alpha_{t|s} \mathbf{x} + (1 - \alpha_{t|s}) \mathbf{1} \mathbf{m}^\top \mathbf{x}] \odot [\alpha_s \mathbf{x} + (1 - \alpha_s) \mathbf{m}]}{\alpha_t \mathbf{x}^\top \mathbf{x} + (1 - \alpha_t) \mathbf{x}^\top \mathbf{m}} \right) \\
 &= \text{Cat} \left(\mathbf{z}_s; \frac{[\alpha_{t|s} \mathbf{x}] \odot [\alpha_s \mathbf{x} + (1 - \alpha_s) \mathbf{m}]}{\alpha_t} \right) \quad \text{since } \mathbf{x}^\top \mathbf{m} = 0 \\
 &= \text{Cat} \left(\mathbf{z}_s; \frac{\alpha_t \mathbf{x}}{\alpha_t} \right) \quad \text{since } \mathbf{x}^\top \mathbf{m} = 0 \text{ and } \alpha_t = \alpha_{t|s} \alpha_s \\
 &= \text{Cat}(\mathbf{z}_s; \mathbf{x}) \quad \text{since } \alpha_t = \alpha_{t|s} \alpha_s \tag{16}
 \end{aligned}$$

Thus, we have the following:

$$q(\mathbf{z}_s | \mathbf{z}_t = \mathbf{x}, \mathbf{x}) = \text{Cat}(\mathbf{z}_s; \mathbf{x}). \tag{17}$$

Case 2. Consider the case $\mathbf{z}_t = \mathbf{m}$. By substituting $\mathbf{z}_t = \mathbf{m}$ and $\pi = \mathbf{m}$ in (14), $q(\mathbf{z}_s | \mathbf{z}_t, \mathbf{x})$ simplifies to the following:

$$\begin{aligned}
 q(\mathbf{z}_s | \mathbf{z}_t = \mathbf{m}, \mathbf{x}) &= \text{Cat} \left(\frac{(\alpha_{t|s} \mathbf{m} + (1 - \alpha_{t|s}) \mathbf{1}) \odot (\alpha_s \mathbf{x} + (1 - \alpha_s) \mathbf{m})}{(1 - \alpha_t)} \right) \\
 &= \text{Cat} \left(\frac{(\alpha_{t|s} (1 - \alpha_s) \mathbf{m} + (1 - \alpha_{t|s}) (1 - \alpha_s) \mathbf{m} + (\alpha_s - \alpha_t) \mathbf{x})}{(1 - \alpha_t)} \right) \\
 &= \text{Cat} \left(\mathbf{z}_s; \frac{(1 - \alpha_s) \mathbf{m} + (\alpha_s - \alpha_t) \mathbf{x}}{1 - \alpha_t} \right) \tag{18}
 \end{aligned}$$

Note that the above categorical distribution is non-zero for $\mathbf{z}_s \in \{\mathbf{x}, \mathbf{m}\}$ and zero for every other value. The non-zero values are specified as follows:

$$q(\mathbf{z}_s = \mathbf{x} | \mathbf{z}_t = \mathbf{m}, \mathbf{x}) = \frac{\alpha_s - \alpha_t}{1 - \alpha_t} \tag{19}$$

$$q(\mathbf{z}_s = \mathbf{m} | \mathbf{z}_t = \mathbf{m}, \mathbf{x}) = \frac{1 - \alpha_s}{1 - \alpha_t} \tag{20}$$

A.3.2. $p_\theta(\mathbf{z}_s | \mathbf{z}_t)$

For the absorbing state diffusion process with $\pi = \mathbf{m}$, we want to simplify the (15). For this reason, we consider 2 cases: first, when $\mathbf{z}_t \neq \mathbf{m}$ (**case 1**), second, when $\mathbf{z}_t = \mathbf{m}$ (**case 2**).

Case 1. Consider the case when $\mathbf{z}_t \neq \mathbf{m}$. (15) simplifies to the following:

$$p_\theta(\mathbf{z}_s | \mathbf{z}_t \neq \mathbf{m}) = \text{Cat} \left(\mathbf{x}_s; \frac{\bar{Q}_{t|s} \mathbf{z}_t \odot \bar{Q}_s^\top \mathbf{x}_\theta(\mathbf{z}_t, t)}{\mathbf{z}_t^\top \bar{Q}_t^\top \mathbf{x}_\theta(\mathbf{z}_t, t)} \right) \quad (21)$$

$$\begin{aligned} &= \text{Cat} \left(\mathbf{x}_s; \frac{\bar{Q}_{t|s} \mathbf{z}_t \odot \bar{Q}_s^\top \mathbf{x}_\theta(\mathbf{z}_t, t)}{[\bar{Q}_t \mathbf{z}_t]^\top \mathbf{x}_\theta(\mathbf{z}_t, t)} \right) \\ &= \text{Cat} \left(\mathbf{x}_s; \frac{[\alpha_t | \mathbf{z}_t] \odot [\alpha_s \mathbf{I}_n + (1 - \alpha_s) \mathbf{m} \mathbf{1}^\top] \mathbf{x}_\theta(\mathbf{z}_t, t)}{[\alpha_t \mathbf{z}_t]^\top \mathbf{x}_\theta(\mathbf{z}_t, t)} \right) \\ &= \text{Cat} \left(\mathbf{x}_s; \frac{[\alpha_t | \mathbf{z}_t] \odot [\alpha_s \mathbf{x}_\theta(\mathbf{z}_t, t) + (1 - \alpha_s) \mathbf{m} \langle \mathbf{1}, \mathbf{x}_\theta(\mathbf{z}_t, t) \rangle]}{\alpha_t \langle \mathbf{z}_t, \mathbf{x}_\theta(\mathbf{z}_t, t) \rangle} \right) \end{aligned}$$

since $\langle \mathbf{1}, \mathbf{x}_\theta(\mathbf{z}_t, t) \rangle = 1$, we have the following:

$$= \text{Cat} \left(\mathbf{x}_s; \frac{[\alpha_t | \mathbf{z}_t] \odot [\alpha_s \mathbf{x}_\theta(\mathbf{z}_t, t) + (1 - \alpha_s) \mathbf{m}]}{\alpha_t \langle \mathbf{z}_t, \mathbf{x}_\theta(\mathbf{z}_t, t) \rangle} \right)$$

since $\mathbf{z}_t \odot \mathbf{m} = \mathbf{0}$, we have the following:

$$= \text{Cat} \left(\mathbf{x}_s; \frac{\alpha_t \mathbf{z}_t \odot \mathbf{x}_\theta(\mathbf{z}_t, t)}{\alpha_t \langle \mathbf{z}_t, \mathbf{x}_\theta(\mathbf{z}_t, t) \rangle} \right) \quad (22)$$

Case 2. Consider the case when $\mathbf{z}_t = \mathbf{m}$. (15) simplifies to the following:

$$\begin{aligned} p_\theta(\mathbf{x}_s | \mathbf{z}_t = \mathbf{m}) &= \text{Cat} \left(\mathbf{x}_s; \frac{\bar{Q}_{t|s} \mathbf{m} \odot \bar{Q}_s^\top \mathbf{x}_\theta(\mathbf{z}_t, t)}{\mathbf{m}^\top \bar{Q}_t^\top \mathbf{x}_\theta(\mathbf{z}_t, t)} \right) \\ &= \text{Cat} \left(\mathbf{x}_s; \frac{\bar{Q}_{t|s} \mathbf{m} \odot \bar{Q}_s^\top \mathbf{x}_\theta(\mathbf{z}_t, t)}{[\bar{Q}_t^\top \mathbf{m}]^\top \mathbf{x}_\theta(\mathbf{z}_t, t)} \right) \\ &= \text{Cat} \left(\mathbf{x}_s; \frac{[\alpha_t | \mathbf{m} + (1 - \alpha_t) \mathbf{1}] \odot [\alpha_s \mathbf{I}_n + (1 - \alpha_s) \mathbf{m} \mathbf{1}^\top] \mathbf{x}_\theta(\mathbf{z}_t, t)}{[\alpha_t \mathbf{m} + (1 - \alpha_t) \mathbf{1}]^\top \mathbf{x}_\theta(\mathbf{z}_t, t)} \right) \\ &= \text{Cat} \left(\mathbf{x}_s; \frac{[\alpha_t | \mathbf{m} + (1 - \alpha_t) \mathbf{1}] \odot [\alpha_s \mathbf{x}_\theta(\mathbf{z}_t, t) + (1 - \alpha_s) \mathbf{m} \langle \mathbf{1}, \mathbf{x}_\theta(\mathbf{z}_t, t) \rangle]}{\alpha_t \langle \mathbf{m}, \mathbf{x}_\theta(\mathbf{z}_t, t) \rangle + (1 - \alpha_t) \langle \mathbf{1}, \mathbf{x}_\theta(\mathbf{z}_t, t) \rangle} \right) \\ &= \text{Cat} \left(\mathbf{x}_s; \frac{[\alpha_t | \mathbf{m} + (1 - \alpha_t) \mathbf{1}] \odot [\alpha_s \mathbf{x}_\theta(\mathbf{z}_t, t) + (1 - \alpha_s) \mathbf{m}]}{\alpha_t \langle \mathbf{x}_\theta(\mathbf{z}_t, t), \mathbf{m} \rangle + (1 - \alpha_t)} \right) \\ &= \text{Cat} \left(\mathbf{x}_s; \frac{\alpha_t \mathbf{m} \odot \mathbf{x}_\theta(\mathbf{z}_t, t) + (\alpha_s - \alpha_t) \mathbf{x}_\theta(\mathbf{z}_t, t) + (1 - \alpha_s) \mathbf{m}}{\alpha_t \langle \mathbf{x}_\theta(\mathbf{z}_t, t), \mathbf{m} \rangle + (1 - \alpha_t)} \right) \end{aligned} \quad (23)$$

Note that the above categorical distribution, we can obtain the values for $p_\theta(\mathbf{x}_s = \mathbf{x} | \mathbf{x}_t = \mathbf{m})$ and $p_\theta(\mathbf{x}_s = \mathbf{m} | \mathbf{x}_t = \mathbf{m})$ which are as follows:

$$p_\theta(\mathbf{x}_s = \mathbf{x} | \mathbf{x}_t = \mathbf{m}) = \frac{(\alpha_s - \alpha_t) \langle \mathbf{x}_\theta(\mathbf{z}_t, t), \mathbf{x} \rangle}{\alpha_t \langle \mathbf{x}_\theta(\mathbf{z}_t, t), \mathbf{m} \rangle + (1 - \alpha_t)} \quad (24)$$

$$p_\theta(\mathbf{x}_s = \mathbf{m} | \mathbf{x}_t = \mathbf{m}) = \frac{\alpha_s \langle \mathbf{x}_\theta(\mathbf{z}_t, t), \mathbf{m} \rangle + (1 - \alpha_s)}{\alpha_t \langle \mathbf{x}_\theta(\mathbf{z}_t, t), \mathbf{m} \rangle + (1 - \alpha_t)} \quad (25)$$

As a sanity check, we can verify that (24) reduces to (19), and (25) reduces to (20) if our denoising network can reconstruct \mathbf{x} perfectly, i.e., $\mathbf{x}_\theta(\mathbf{z}_t, t) = \mathbf{x}$.

A.3.3. DIFFUSION LOSS

For a given T , Let $\mathcal{L}_T = \mathbb{E}_{t \in \{1, \dots, T\}} \mathbb{E}_{q(\mathbf{x}_t | \mathbf{x})} TD_{\text{KL}}(q(\mathbf{x}_s | \mathbf{x}_t, \mathbf{x}) || p_\theta(\mathbf{x}_s | \mathbf{x}_t))$ denote the diffusion loss. We break down the computation of $D_{\text{KL}}(q(\mathbf{x}_s | \mathbf{x}_t, \mathbf{x}) || p_\theta(\mathbf{x}_s | \mathbf{x}_t))$ into 2 cases: $\mathbf{z}_t = \mathbf{x}$ (**case 1**) and $\mathbf{z}_t = \mathbf{m}$ (**case 2**).

Case 1. consider the case $\mathbf{z}_t = \mathbf{x}$. Let's simplify $D_{\text{KL}}(q(\mathbf{z}_s | \mathbf{z}_t = \mathbf{x}, \mathbf{x}) || p_\theta(\mathbf{z}_s | \mathbf{z}_t = \mathbf{x}))$.

$$\begin{aligned}
 & \mathbb{D}_{\text{KL}}(q(\mathbf{z}_s | \mathbf{z}_t = \mathbf{x}, \mathbf{x}) \| p_\theta(\mathbf{z}_s | \mathbf{z}_t = \mathbf{x})) \\
 &= \sum_{\mathbf{z}_s} q(\mathbf{z}_s | \mathbf{z}_t = \mathbf{x}, \mathbf{x}) \log \frac{q(\mathbf{z}_s | \mathbf{z}_t = \mathbf{x}, \mathbf{x})}{p_\theta(\mathbf{z}_s | \mathbf{z}_t = \mathbf{x})} \\
 & \text{Since } q(\mathbf{z}_s | \mathbf{z}_t, \mathbf{x}) \text{ is 1 only for } \mathbf{z}_s = \mathbf{x} \text{ we get,} \\
 &= \log \frac{1}{p_\theta(\mathbf{z}_s = \mathbf{x} | \mathbf{z}_t = \mathbf{x})} \\
 &= \log 1 \quad \text{From (21)} \\
 &= 0 \quad (26)
 \end{aligned}$$

Case 2. Consider the case $\mathbf{z}_t = \mathbf{m}$. Let's simplify $\mathbb{D}_{\text{KL}}(q(\mathbf{x}_s | \mathbf{x}_t = \mathbf{m}, \mathbf{x}) \| p_\theta(\mathbf{x}_s | \mathbf{x}_t = \mathbf{m}))$.

$$\begin{aligned}
 & \mathbb{D}_{\text{KL}}(q(\mathbf{x}_s | \mathbf{x}_t = \mathbf{m}, \mathbf{x}) \| p_\theta(\mathbf{x}_s | \mathbf{x}_t = \mathbf{m})) \\
 &= \sum_{\mathbf{x}_s} q(\mathbf{x}_s | \mathbf{x}_t = \mathbf{m}, \mathbf{x}) \log \frac{q(\mathbf{x}_s | \mathbf{x}_t = \mathbf{m}, \mathbf{x})}{p_\theta(\mathbf{x}_s | \mathbf{x}_t = \mathbf{m})} \\
 &= \sum_{\mathbf{x}_s \in \{\mathbf{x}, \mathbf{m}\}} q(\mathbf{x}_s | \mathbf{x}_t = \mathbf{m}, \mathbf{x}) \log \frac{q(\mathbf{x}_s | \mathbf{x}_t = \mathbf{m}, \mathbf{x})}{p_\theta(\mathbf{x}_s | \mathbf{x}_t = \mathbf{m})} \\
 &= \underbrace{q(\mathbf{x}_s = \mathbf{x} | \mathbf{x}_t = \mathbf{m}, \mathbf{x}) \log \frac{q(\mathbf{x}_s = \mathbf{x} | \mathbf{x}_t = \mathbf{m}, \mathbf{x})}{p_\theta(\mathbf{x}_s = \mathbf{x} | \mathbf{x}_t = \mathbf{m})}}_{\text{Simplify using (19) and (24)}} \\
 &+ \underbrace{q(\mathbf{x}_s = \mathbf{m} | \mathbf{x}_t = \mathbf{m}, \mathbf{x}) \log \frac{q(\mathbf{x}_s = \mathbf{m} | \mathbf{x}_t = \mathbf{m}, \mathbf{x})}{p_\theta(\mathbf{x}_s = \mathbf{m} | \mathbf{x}_t = \mathbf{m})}}_{\text{Simplify using (20) and (25)}} \\
 &= \frac{\alpha_s - \alpha_t}{1 - \alpha_t} \log \frac{\alpha_t \langle \mathbf{x}_\theta(\mathbf{z}_t), \mathbf{m} \rangle + (1 - \alpha_t)}{(1 - \alpha_t) \langle \mathbf{x}_\theta(\mathbf{z}_t), \mathbf{x} \rangle} \\
 &+ \frac{1 - \alpha_s}{1 - \alpha_t} \log \frac{(1 - \alpha_s) (\alpha_t \langle \mathbf{x}_\theta(\mathbf{z}_t), \mathbf{m} \rangle + (1 - \alpha_t))}{(1 - \alpha_t) (\alpha_s \langle \mathbf{x}_\theta(\mathbf{z}_t), \mathbf{m} \rangle + (1 - \alpha_s))} \quad (27)
 \end{aligned}$$

Thus, $\mathbb{D}_{\text{KL}}(q(\mathbf{x}_s | \mathbf{x}_t, \mathbf{x}) \| p_\theta(\mathbf{x}_s | \mathbf{x}_t))$ can be written in the following manner where $\langle \mathbf{z}_t, \mathbf{x}_0 \rangle$ evaluates to 1 if $\mathbf{z}_t = \mathbf{x}$ and $\langle \mathbf{z}_t, \mathbf{m} \rangle$ evaluates to 1 if $\mathbf{z}_t = \mathbf{m}$:

$$\begin{aligned}
 & \mathbb{D}_{\text{KL}}(q(\mathbf{x}_s | \mathbf{x}_t, \mathbf{x}) \| p_\theta(\mathbf{x}_s | \mathbf{x}_t)) \\
 &= \underbrace{\mathbb{D}_{\text{KL}}(q(\mathbf{x}_s | \mathbf{x}_t = \mathbf{x}, \mathbf{x}) \| p_\theta(\mathbf{x}_s | \mathbf{x}_t = \mathbf{x}))}_{=0, \text{ from (26)}} \langle \mathbf{z}_t, \mathbf{x}_0 \rangle + \underbrace{\mathbb{D}_{\text{KL}}(q(\mathbf{x}_s | \mathbf{x}_t = \mathbf{m}, \mathbf{x}) \| p_\theta(\mathbf{x}_s | \mathbf{x}_t = \mathbf{m}))}_{\text{Given by (27)}} \langle \mathbf{z}_t, \mathbf{m} \rangle \quad (28)
 \end{aligned}$$

Thus, we derive the diffusion loss, \mathcal{L}_T , in the following manner:

$$\begin{aligned}
 \mathcal{L}_T &= \mathbb{E}_{t \in \{1, \dots, T\}} \mathbb{E}_{q(\mathbf{x}_t | \mathbf{x})} T \mathbb{D}_{\text{KL}}(q(\mathbf{x}_s | \mathbf{x}_t, \mathbf{x}) \| p_\theta(\mathbf{x}_s | \mathbf{x}_t)) \\
 &= \mathbb{E}_{t \in \{1, \dots, T\}} \mathbb{E}_{q(\mathbf{x}_t | \mathbf{x})} T \left[\frac{\alpha_s - \alpha_t}{1 - \alpha_t} \log \frac{\alpha_t \langle \mathbf{x}_\theta(\mathbf{z}_t), \mathbf{m} \rangle + (1 - \alpha_t)}{(1 - \alpha_t) \langle \mathbf{x}_\theta(\mathbf{z}_t), \mathbf{x} \rangle} \right. \\
 &\quad \left. + \frac{1 - \alpha_s}{1 - \alpha_t} \log \frac{(1 - \alpha_s) (\alpha_t \langle \mathbf{x}_\theta(\mathbf{z}_t), \mathbf{m} \rangle + (1 - \alpha_t))}{(1 - \alpha_t) (\alpha_s \langle \mathbf{x}_\theta(\mathbf{z}_t), \mathbf{m} \rangle + (1 - \alpha_s))} \right] \langle \mathbf{z}_t, \mathbf{m} \rangle \quad (29)
 \end{aligned}$$

Note that \mathcal{L}_T is 0 if \mathbf{z}_t is an unmasked token i.e. $\mathbf{z}_t = \mathbf{x}$.

B. MDLM: Rao-Blackwelization using SUBS parameterization

In this section we show how SUBS parameterization can simplify the functional form of the ELBO as defined in (29).

B.1. ELBO

The SUBS parameterization, as described in Sec. 3.2, simplifies $D_{\text{KL}}(q(\mathbf{x}_s|\mathbf{x}_t=\mathbf{m},\mathbf{x})\|p_\theta(\mathbf{x}_s|\mathbf{x}_t=\mathbf{m}))$ ((27)) to the following:

$$\begin{aligned} & D_{\text{KL}}(q(\mathbf{x}_s|\mathbf{x}_t=\mathbf{m},\mathbf{x})\|p_\theta(\mathbf{x}_s|\mathbf{x}_t=\mathbf{m})) \\ &= \frac{\alpha_s - \alpha_t}{1 - \alpha_t} \log \frac{\alpha_t \langle \mathbf{x}_\theta(\mathbf{z}_t), \mathbf{m} \rangle + (1 - \alpha_t)}{(1 - \alpha_t) \langle \mathbf{x}_\theta(\mathbf{z}_t), \mathbf{x} \rangle} \\ &+ \frac{1 - \alpha_s}{1 - \alpha_t} \log \frac{(1 - \alpha_s) (\alpha_t \langle \mathbf{x}_\theta(\mathbf{z}_t), \mathbf{m} \rangle + (1 - \alpha_t))}{(1 - \alpha_t) (\alpha_s \langle \mathbf{x}_\theta(\mathbf{z}_t), \mathbf{m} \rangle + (1 - \alpha_s))} \end{aligned}$$

Since SUBS sets $\langle \mathbf{x}_\theta(\mathbf{z}_t), \mathbf{m} \rangle = 0$, the above equation simplifies to the following:

$$\begin{aligned} &= \frac{\alpha_s - \alpha_t}{1 - \alpha_t} \log \frac{(1 - \alpha_t)}{(1 - \alpha_t) \langle \mathbf{x}_\theta(\mathbf{z}_t), \mathbf{x} \rangle} \\ &= \frac{\alpha_t - \alpha_s}{1 - \alpha_t} \log \langle \mathbf{x}_\theta(\mathbf{z}_t), \mathbf{x} \rangle \end{aligned} \tag{30}$$

Using this, we obtain the following expression for the diffusion loss, \mathcal{L}_T :

$$\begin{aligned} \mathcal{L}_T &= T \mathbb{E}_{t \in \{1, \dots, T\}} \mathbb{E}_{q(\mathbf{x}_t|\mathbf{x})} D_{\text{KL}}(q(\mathbf{x}_s|\mathbf{x}_t=\mathbf{m},\mathbf{x})\|p_\theta(\mathbf{x}_s|\mathbf{x}_t=\mathbf{m})) \langle \mathbf{z}_t, \mathbf{m} \rangle \\ &= T \mathbb{E}_{t \in \{1, \dots, T\}} \mathbb{E}_{q(\mathbf{x}_t|\mathbf{x})} \frac{\alpha_t - \alpha_s}{1 - \alpha_t} \log \langle \mathbf{x}_\theta(\mathbf{z}_t), \mathbf{x} \rangle \langle \mathbf{z}_t, \mathbf{m} \rangle \end{aligned}$$

When $\mathbf{z}_t = \mathbf{m}$, $\log \langle \mathbf{x}_\theta(\mathbf{z}_t), \mathbf{x} \rangle = 0$; hence, the term $\langle \mathbf{z}_t, \mathbf{m} \rangle$ can be safely dropped to obtain:

$$= T \mathbb{E}_{t \in \{1, \dots, T\}} \mathbb{E}_{q(\mathbf{x}_t|\mathbf{x})} \frac{\alpha_t - \alpha_s}{1 - \alpha_t} \log \langle \mathbf{x}_\theta(\mathbf{z}_t), \mathbf{x} \rangle \tag{31}$$

B.2. Continuous Time ELBO

To derive the continuous-time diffusion loss, $\mathcal{L}_{\text{diffusion}}^\infty$, we consider the limiting case $\lim_{T \rightarrow \infty} \mathcal{L}_T$:

$$\begin{aligned} \mathcal{L}_{\text{diffusion}}^\infty &= \lim_{T \rightarrow \infty} \mathcal{L}_T \\ &= \mathbb{E}_{t \in \{1, \dots, T\}} \mathbb{E}_{q(\mathbf{x}_t|\mathbf{x})} \left[\lim_{T \rightarrow \infty} T \frac{\alpha_t - \alpha_s}{1 - \alpha_t} \log \langle \mathbf{x}_\theta(\mathbf{z}_t), \mathbf{x} \rangle \right] \end{aligned}$$

Using $\lim_{T \rightarrow \infty} T(\alpha_s - \alpha_t) = \alpha'_t$, we obtain:

$$= \mathbb{E}_{t \sim [0, 1]} \mathbb{E}_{q(\mathbf{x}_t|\mathbf{x})} \left[\frac{\alpha'_t}{1 - \alpha_t} \log \langle \mathbf{x}_\theta(\mathbf{z}_t), \mathbf{x} \rangle \right] \tag{32}$$

C. Additional Experiments

C.1. Experimental Setup

We evaluate MDLM as a generative model of language and as a representation model via fine-tuning on downstream tasks.

For language modeling likelihood evaluation, we conduct experiments on two datasets: The One Billion Words Dataset (LM1B; (Chelba et al., 2014)) and OpenWebText (OWT; (Gokaslan et al., 2019)). We use the `bert-base-uncased` tokenizer for One Billion Words, and report perplexities on the test split. Models have a context size of 128. For OWT, which does not have a pre-defined split, we reserve the last 100K documents as a held-out validation set and report perplexities on this set. We use the `GPT2` tokenizer (Radford et al., 2019) for OWT. Models have a context size of 1,024. We utilize the transformer architecture from Lou et al. (2023), which augments the diffusion transformer (Peebles & Xie, 2023) with rotary embeddings (Su et al., 2021). MDLM was trained for 1M or 10M steps (corresponding to 33B, 330B tokens, respectively) on LM1B and 1M steps on OWT (which corresponds to 262B tokens). The corresponding AR baseline was trained for half the number of steps to ensure similar number of tokens seen (details in Suppl. F). Full hyperparameters are given in Suppl. I.1. On OWT, we train with and without time step conditioning.

For representation learning, we pre-train models on the C4 dataset (Raffel et al., 2020), then fine-tune and evaluate models on the GLUE benchmark (Wang et al., 2019). Models have a context size of 128. We use the `bert-base-uncased` tokenizer for the representation learning experiments. We utilize the MosaicBERT architecture from Portes et al. (2024), an extension of the original BERT architecture (Devlin et al., 2018). We pre-train a bidirectional MosaicBERT using an MLM objective for 37B tokens of C4, as well as a causal variant on the same data. We further fine-tune MosaicBERT model using the MDLM for 327M tokens, less than 1% of the pre-training data. We provide the full hyperparameters in Suppl. I.3.

C.2. LM1B perplexity

Table 4: Test perplexities (PPL; \downarrow) on LM1B. \dagger Reported in He et al. (2022). Best diffusion value is bolded.

		Parameters	PPL (\downarrow)
<i>Autoregressive</i>	Transformer-X Base (Dai et al., 2019)	0.46B	23.5
	OmniNet _T (Tay et al., 2021)	100M	21.5
<i>Diffusion</i>	BERT-Mouth (Wang & Cho, 2019)	110M	≤ 142.89
	D3PM (absorb) (Austin et al., 2021)	70M	≤ 77.50
	Diffusion-LM (Li et al., 2022) \dagger	80M	≤ 118.62
	DiffusionBert (He et al., 2022)	110M	≤ 63.78
	SEDD (Lou et al., 2023) (33B tokens)	110M	≤ 32.79
<i>Autoregressive (Retrained)</i>	Transformer (33B tokens)	110M	22.32
	Transformer (330B tokens)		20.86
<i>Diffusion (Ours)</i>	MDLM (33B tokens)	110M	≤ 27.04
	MDLM (330B tokens)		$\leq \mathbf{23.00}$

C.3. LM1B ablations

We assess the importance of our continuous-time framework by performing ablation on diffusion steps T . In Table 5, we compare NLL and PPL under continuous and discrete T in MDLM. We find that NLL consistently decreases as $T \rightarrow \infty$.

Table 5: Discrete vs continuous time evaluation for MDLM on LM1B. MDLM was trained with $T = \infty$ and a smaller model containing 70M non-embedding parameters for 200K steps. We report test perplexity for a discrete T .

Method	NLL	PPL
MDLM _{$T=\infty$}	$\leq \mathbf{3.61 \pm 0.001}$	$\leq \mathbf{37.25}$
MDLM _{$T=10$}	$\leq 4.14 \pm 0.003$	≤ 62.83
MDLM _{$T=100$}	$\leq 3.66 \pm 0.002$	≤ 39.04
MDLM _{$T=1000$}	$\leq 3.62 \pm 0.000$	≤ 37.38

C.4. Train NLL curves on OWT

In Figure 2, we show that MDLM achieves lower variance loss during training compared to a previous diffusion language model, SEDD. Training is performed over 1M steps on OWT (which corresponds to 524B tokens).

C.5. Time-conditioning ablation on OWT

In Table 6, we assess the importance of time conditioning in MDLM on OWT. We observe that time-conditioning has minimal impact on perplexity. Training is performed over 1M steps on OWT (which corresponds to 524B tokens).

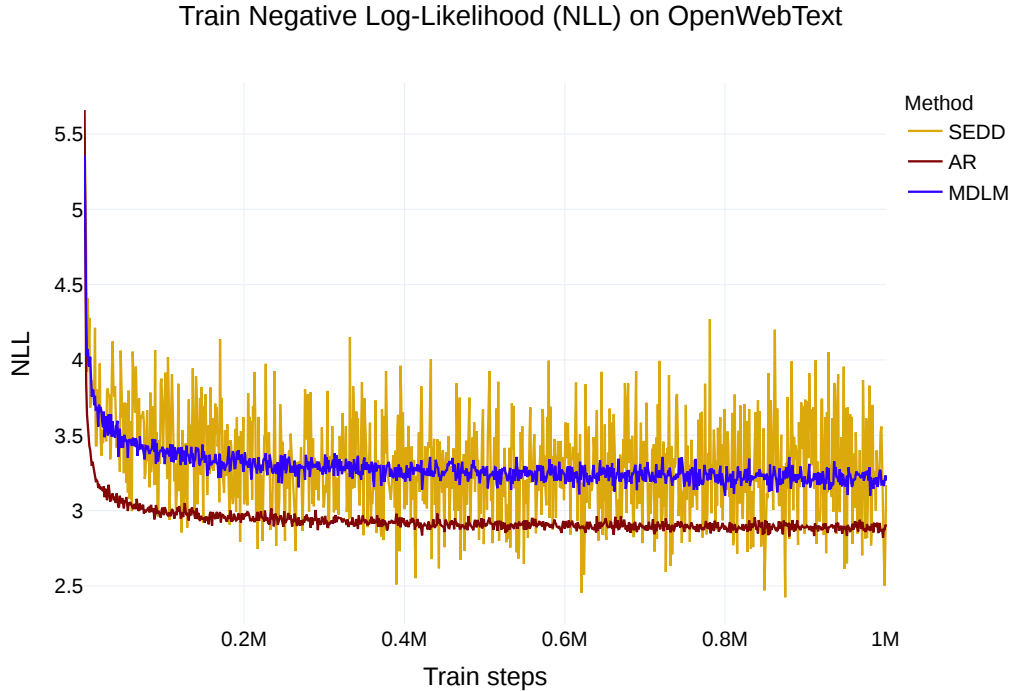


Figure 2: Train negative log-likelihood (NLL) curves across 1M gradient steps (524B tokens) on OpenWebText (Gokaslan et al., 2019). NLL is logged every 1K steps without value smoothing.

Table 6: Ablation on time-conditioning in MDLM on OWT.

Method	PPL
MDLM w/ time-conditioning	23.21
MDLM w/o time-conditioning	23.05

C.6. Zero shot evaluations

We also explore models’ ability to generalize by taking models trained on OWT and evaluating how well they model unseen datasets. We compare the perplexities of our MDLM with a SEDD parameterization and an AR Transformer language model. Our zero-shot datasets include the validation splits of Penn Tree Bank (PTB; (Marcus et al., 1993)), Wikitext (Merity et al., 2016), LM1B, Lambada (Paperno et al., 2016), AG News (Zhang et al., 2015), and Scientific Papers (Pubmed and Arxiv subsets; (Cohan et al., 2018)). Full experimental details are available in Suppl. I.1.

MDLM consistently outperforms the SEDD diffusion parameterization. In some cases, e.g., for Lambada and Scientific Papers, MDLM attains better perplexity than AR. We hypothesize that these datasets are farther from OWT, and that diffusion models may be more robust to out-of-domain evaluation due to the unmasking-based objective.

Table 7: Zero-shot validation perplexities (\downarrow) of models trained for 524B tokens on OWT. All perplexities for diffusion models are upper bounds.

	PTB	Wikitext	LM1B	Lambada	AG News	Pubmed	Arxiv
AR (Retrained)	82.05	25.75	51.25	51.28	52.09	49.01	41.73
SEDD (Retrained)	100.09	34.28	68.20	49.86	62.09	44.53	38.48
MDLM (Ours)	95.26	32.83	67.01	47.52	61.15	41.89	37.37

C.7. Glue Evaluation

Table 8: GLUE evaluation results. Evaluation measures (\uparrow) are F1 score for QQP and MRPC, Spearman correlations for STS-B, and accuracy for the rest. For MNLI, we report match/mismatch accuracies.

	MNLI (m/mm)	QQP	QNLI	SST-2	COLA	STS-B	MRPC	RTE	Avg
AR	80.94/80.78	86.98	86.16	90.14	33.43	84.32	83.88	47.29	74.88
BERT	84.43/85.35	88.41	90.46	92.20	54.81	88.41	89.16	61.37	81.62
+MDLM-FT	84.76/85.07	88.49	90.30	92.20	57.69	87.48	90.53	62.09	82.06

C.8. OWT perplexity

Table 9: Test perplexities (PPL; \downarrow) on OWT for models trained for 262B tokens. \dagger denotes retrained models.

	PPL (\downarrow)
AR \dagger	17.54
SEDD \dagger	≤ 24.10
MDLM (Ours)	$\leq \mathbf{23.21}$

C.9. Ablation Analysis

Table 10: Test perplexities (PPL; \downarrow) for MDLM ablations on LM1B. All the models were trained for 200K steps. Standard deviation is measured over 5 seeds during evaluation.

	PPL
MDLM	33.59 \pm .11
w/o Continuous time	33.70 \pm .07
& carry-over	35.57 \pm .15
& zero masking	35.31 \pm .16

In Table 10, we can see the effect of our streamlined masked diffusion implementation. The improvements described in Sec. ?? allow us to greatly reduce perplexity of previously discounted models, such as D3PM (see the bottom row of this table, which is mathematically equivalent to the D3PM formulation). While most works assumed that D3PM achieves mediocre log-likelihoods, we show that is is incorrect: our re-implementation almost matches state-of-the-art score-based methods. This introduces a new strong baseline that opens new research opportunities. Additionally, in Table 10, we ablate different components of MDLM. We observe that the perplexity for MDLM trained with a discrete $T = 1000$ marginally worsens by 0.1 compared to MDLM trained in continuous time. Additionally, removing the “carry over” operation from the SUBS parameterization increases the perplexity by 2 points. However, further removing the “zero masking” operation does not lead to any meaningful change in perplexity.

We provide further ablations for the continuous time formulation in the Appendix, showing in Table 5 that for a pre-trained model, at inference, increasing T yields better likelihoods.

C.10. SEMI-AR

To test the SAR decoding algorithm presented in Sec. 4.2, we compare to SSD-LM (Han et al., 2022) a diffusion model that was designed to generate blocks of text autoregressively. We generate 200 sequences of length 2048 tokens on a single 3090 GPU and evaluate generative perplexity under a pre-trained GPT-2 (Radford et al., 2019) model. The SSD-LM sequences are generated using blocks of 25 tokens (as implemented in their pre-trained model) and the MDLM sequences are generated using $L' = 512$. In Table 11, we find that in addition to achieving better generative perplexity, MDLM enables ~ 25 -30x faster SAR decoding relative to SSD-LM.

Table 11: Semi-AR generative perplexity (Gen. PPL; \downarrow) for sequences of 2048 tokens.

	Gen. PPL (\downarrow)	Sec/Seq (\downarrow)
SSD-LM	35.43	2473.9
MDLM (Ours)	27.18	89.3

C.11. Generative Performance

Table 12: Test perplexities (PPL; \downarrow) of generative fine-tuning of the Caduceus MLM (Schiff et al., 2024) on the HG38 reference genome. Best diffusion model values are bolded. Error bars indicate the difference between the maximum and minimum values across 5 random seeds used for fine-tuning. \dagger denotes retrained models.

		Params	PPL (\downarrow)
AR^\dagger	Mamba	465K	$3.067 \pm .0104$
	HyenaDNA	433K	$3.153 \pm .001$
Dif^\dagger	Plaid	507K	$\leq 3.240 \pm .005$
	SEDD	467K	$\leq 3.216 \pm .003$
$Dif(Ours)$	MDLM	467K	$\leq \mathbf{3.199} \pm .010$

D. Noise schedule parameterization

As described in Sec. 3.4, the ELBO is invariant to the functional form of α_t . To demonstrate this, we evaluate MDLM, initially trained using a log-linear schedule on OWT, by replacing the noise schedule with various other noise schedules as mentioned below. Following prior works (Austin et al., 2021; Lou et al., 2023; Sohl-Dickstein et al., 2015), we parameterize $\alpha_t = e^{-\sigma(t)}$, where $\sigma(t) : [0,1] \rightarrow \mathbb{R}^+$. Various functional forms of $\sigma(t)$ are listed below:

Log Linear (Austin et al., 2021; Lou et al., 2023; Sohl-Dickstein et al., 2015) The log linear schedule is given as:

$$\sigma(t) = -\log t \quad (33)$$

Cosine Squared schedule (Han et al., 2022) The Cosine Squared schedule is given as:

$$\sigma(t) = -\log \cos^2 \left(\frac{\pi}{2} (1-t) \right) \quad (34)$$

Cosine schedule The Cosine schedule is given as:

$$\sigma(t) = -\log \cos^2 \left(\frac{\pi}{2} (1-t) \right) \quad (35)$$

Linear The Linear schedule is given as:

$$\sigma(t) = \sigma_{\max} (1-t) \quad (36)$$

where σ_{\max} is a very large number. In our experiments we set it to 10^8 .

In Table 13 we demonstrate empirically that noise schedules with different functional forms evaluate to the same Likelihood which is consistent with our theory in Sec. 3.4. However, different schedules lead to different per data point variance.

E. Likelihood Evaluation

How you do it Say that it incurs lower variance by referencing to the Ablations table The variance is low because of the low discrepancy sampler

Table 13: Likelihood in bits per dimension (BPD) for different noise schedules on OWT dataset, is reported along with the mean and variance associated with each noise schedule per data point. We empirically observe that noise schedules with different functional forms yield the same likelihood, consistent with our theory in Sec. 3.4; however, different schedules result in different variances. Notably, the log-linear schedule exhibits the lowest variance among all the noise schedules considered.

$\sigma(t)$	Mean	Variance per datapoint
Log Linear (33)	3.30	1.81
Cosine (35)	3.30	3.30
Cosine Squared (34)	3.30	3.30
Linear (36)	3.30	7.57

F. Avg. Number of Tokens seen

Given `training_steps`, `batch_size`, `context_length`, the number of tokens seen by the AR model is given as:

$$\text{training_steps} \times \text{batch_size} \times \text{context_length}.$$

However, this expression doesn't hold true for a diffusion model, since at each training step, the model sees masked input. Let p_m be the probability of a token being masked at a timestep t . Then the diffusion model sees the following number of tokens in expectation:

$$\begin{aligned} & \mathbb{E}_t[\text{training_steps} \times \text{batch_size} \times \text{context_length} \times p_m] \\ &= \text{training_steps} \times \text{batch_size} \times \text{context_length} \times \mathbb{E}_t[p_m] \\ & \text{For log-linear schedule used in our experiments } p_m = t; \text{ thus,} \\ &= \text{training_steps} \times \text{batch_size} \times \text{context_length} \times 0.5 \end{aligned} \tag{37}$$

G. Low discrepancy sampler

To reduce variance during training we use a low-discrepancy sampler, similar to that proposed in Kingma et al. (2021). Specifically, when processing a minibatch of N samples, instead of independently sampling N from a uniform distribution, we partition the unit interval and sample the time step for each sequence $i \in \{1, \dots, N\}$ from a different portion of the interval $t_i \sim U[\frac{i-1}{N}, \frac{i}{N}]$. This ensures that our sampled timesteps are more evenly spaced across the interval $[0, 1]$, reducing the variance of the ELBO.

H. Faster sampling with caching

In Figure 14 we compare the wall clock times of various methods: AR, SEDD, MDLM with caching, and MDLM without caching for generating 64 samples on a single GPU. We observe that MDLM without caching yields samples that consistently get better generative perplexity than SEDD. For $T = \{5k, 10k\}$, both SEDD and MDLM get better generative perplexity than the AR model.

Table 14: Wall clock time reported in seconds.

	$T = 5k$	$T = 10k$
MDLM	4215.9	7675.4
+ caching	2407.3	3626.6
Speedup	1.75x	2.12x

I. Experimental details

I.1. Language Modeling

For our forward noise process, we use a log-linear noise schedule similar to Lou et al. (2023).

Generative perplexities across sample times on OpenWebText

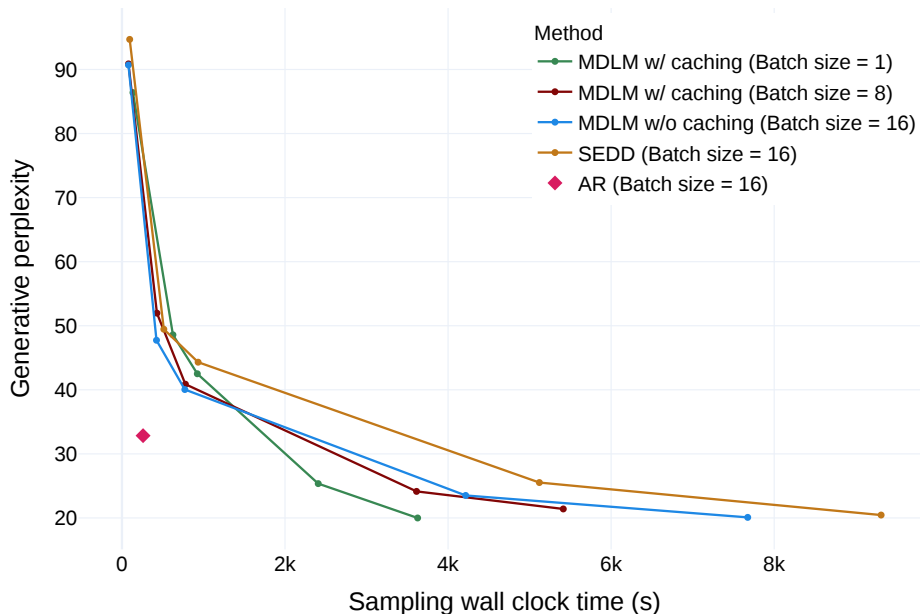


Figure 3: Generative perplexities across wall clock time for generating 64 samples on OWT using a single 32GB A5000 GPU are compared by varying $T \in \{100, 500, 1000, 5000, 10000\}$ in the reverse diffusion process. The samples are generated in mini-batches with a batch size of 16 for AR, SEDD, and MDLM without caching, as it is the largest batch size that fits on this GPU. For MDLM with caching, we vary the batch size.

We detokenize the One Billion Words dataset following Lou et al. (2023), whose code can be found here. We tokenize the One Billion Words dataset with the bert-base-uncased tokenizer, following He et al. (2022). We pad and truncate sequences to a length of 128.

We tokenize OpenWebText with the GPT2 tokenizer. We do not pad or truncate sequences – we concatenate and wrap them to a length of 1,024. When wrapping, we add the eos token in-between concatenated. We additionally set the first and last token of every batch to be eos. Since OpenWebText does not have a validation split, we leave the last 100k docs as validation.

We parameterize our autoregressive baselines, SEDD, and MDLM with the transformer architecture from Lou et al. (2023). We use 12 layers, a hidden dimension of 768, 12 attention heads, and a timestep embedding of 128 when applicable. Word embeddings are not tied between the input and output.

We use the AdamW optimizer with a batch size of 512, constant learning rate warmup from 0 to a learning rate of $3e-4$ for 2,500 steps. We use a constant learning rate for 1M, 5M, or 10M steps on One Billion Words, and 1M steps for OpenWebText. We use a dropout rate of 0.1.

I.2. Zeroshot Likelihood

We evaluate zeroshot likelihoods by taking the models trained on OpenWebText and evaluating likelihoods on the validation splits of 7 datasets: Penn Tree Bank (PTB; Marcus et al. (1993)), Wikitext (Merity et al., 2016), One Billion Word Language Model Benchmark (LM1B; Chelba et al. (2014)), Lambada (Paperno et al., 2016), AG News (Zhang et al., 2015), and Scientific Papers (Pubmed and Arxiv subsets; Cohan et al. (2018)). We detokenize the datasets following Lou et al. (2023). For the AG News and Scientific Papers (Pubmed and Arxiv), we apply both the Wikitext and One Billion Words detokenizers. Since the zeroshot datasets have different conventions for sequence segmentation, we wrap sequences to 1024 and do not add eos tokens in between sequences.

935 I.3. Representation Learning

936 Following [Devlin et al. \(2018\)](#), we evaluate on all GLUE tasks ([Wang et al., 2019](#)), but exclude WNLI.

937 We pre-train a MosaicBERT model on C4 ([Raffel et al., 2020](#)) for 70k steps, corresponding to 36B tokens. We pad and
938 truncate the data to 128 tokens using the `bert-base-uncased` tokenizer.

939 MosaicBERT ([Portes et al., 2024](#)) has a similar architecture to `bert-base-uncased` and has 137M parameters, 12 layers,
940 12 attention heads, a hidden dimension of 768, an intermediate size of 3072, and ALiBi attention bias ([Press et al., 2022](#)).

941 For pre-training, we use the following hyperparameters: A global batch size of 4096 with gradient accumulation, a learning
942 rate of $5e-4$, linear decay to 0.02x of the learning rate with a warmup of 0.06x of the full training duration, and the decoupled
943 AdamW optimizer with $1e-5$ weight decay and betas 0.9 and 0.98.

944 For diffusion fine-tuning we use AdamW with a warmup of 2,500 steps from a learning rate of 0 to $5e-5$, betas 0.95 and 0.999,
945 and batch size 512. We train for 5k steps total, corresponding to 32M tokens.

946 For GLUE evaluation, we use the HuggingFace script found [here](#). We use the default parameters for all datasets, except
947 for a batch size of 16, which we found helped with smaller datasets. This includes the default of 3 epochs for all datasets
948 and learning rate of $2e-5$.

953 I.4. Diffusion DNA Models

954 **Dataset** We pre-train the Caduceus MLM ([Schiff et al., 2024](#)) on the HG38 human reference genome ([Consortium, 2009](#)).
955 Following [Schiff et al. \(2024\)](#), we use character- / base pair-level tokenization. The dataset is based on the splits used in [Avsec
956 et al. \(2021\)](#): the training split comprises of 35 billion tokens covering the human genome. This consists of 34,021 segments
957 extended to a maximum length of 1,048,576 (220 segments). We maintain a constant 2^{20} tokens per batch. For the Genomics
958 Benchmark tasks, we use 5-fold cross-validation where we split the training set into 90/10 train/validation splits.

959 **Architecture** The Caduceus MLM uses as a backbone a bi-directional variant of the data-dependent SSM Mamba block
960 proposed in [Gu et al. \(2021\)](#). This architecture is ideal as it contains inductive biases that preserve reverse complement (RC)
961 equivariance, respecting the inherent symmetry of double-stranded DNA molecules ([Mallet & Vert, 2021](#); [Schiff et al., 2024](#);
962 [Zhou et al., 2022](#)).

963 **Training details** All models are pre-trained on 10B tokens (10K steps) and fine-tuned on a generative objective for an
964 additional 50B tokens (50K steps). We use a global batch size of 1024 for a context length of 1024 tokens. Downstream
965 task fine-tuning is performed for 16K steps (1B tokens).

966 For performing Caduceus MLM pre-training, we follow [Schiff et al. \(2024\)](#) for the model size configuration, and hyperpa-
967 rameter selection. For pre-training, we use a fixed 15% mask rate as done in [Devlin et al. \(2018\)](#). Of the 'masked' tokens,
968 80% are replaced with [MASK], 10% are replaced with a random token from the vocabulary, and 10% are left unchanged.

969 For fine-tuning all Mamba-based models (including Caduceus) on diffusion objectives, we lower the learning rate from $8e-3$ to
970 $1e-3$. For fine-tuning HyenaDNA ([Nguyen et al., 2024](#)), we lower the learning rate from $6e-4$ to $5e-5$. Similar to [Gu et al. \(2021\)](#);
971 [Schiff et al. \(2024\)](#), we found that Mamba-based models were robust to higher learning rates. We exclude timestep embeddings
972 for all Diffusion DNA experiments, as we show it has minimal impact on generative performance (see Table 6, Suppl. C.5).

973 We perform downstream task fine-tuning on the final hidden state embedding from pre-training. We perform mean pooling
974 across the sequence length, which may vary from 200 to approximately 2,000 bps. We report the mean and \pm on max/min
975 classification accuracy over 5-fold cross-validation (CV) using different random seeds, with early stopping on validation
976 accuracy. For each task, we do a hyperparameter sweep over batch size and learning rate and report the values of the 5-fold
977 CV for the best configuration.

978 **Genomic Benchmark Task Distributions** We use a subset of the Genomic Benchmark tasks with an emphasis on tasks
979 from Human data. The positive samples for each dataset were generated by selecting samples that were annotated, either
980 computationally or experimentally, in previous work (e.g enhancers, promoters, open chromatin regions (OCR)) ([Grešová
981 et al., 2023](#)). These annotations each correspond to subsets of the genome of varying sizes that may exhibit different
982 distributions of DNA than those observed globally over the reference genome. Due to this, the observed dataset may have
983 a different distribution than the data used for pre-training and calculating perplexity. This might in turn lead to a case where
984

990 perplexity and downstream performance may not necessarily correlate.

991
992
993
994
995
996
997
998
999
1000
1001
1002
1003
1004
1005
1006
1007
1008
1009
1010
1011
1012
1013
1014
1015
1016
1017
1018
1019
1020
1021
1022
1023
1024
1025
1026
1027
1028
1029
1030
1031
1032
1033
1034
1035
1036
1037
1038
1039
1040
1041
1042
1043
1044